Shaping of metal-organic framework UiO-66 using alginates: effect of operation variables

Daniel W. Lee [1,2]**, Terje Didriksen** [1]**, Unni Olsbye** [2]**, Richard Blom** [1] **and Carlos A. Grande**[1,*]

[1] SINTEF Industry, Forskningsveien 1, 0373. Oslo, Norway

[2] University of Oslo, Institute for Chemistry, P. O. box 1033 Blindern, 0314 Oslo, Norway

* Correspondence:
Corresponding Author: Carlos A. Grande
carlos.grande@sintef.no

Keywords: metal-organic frameworks, MOFs, shaping, alginates, adsorption, UiO-66.

Abstract

Shaping of metal-organic frameworks into macro-structured particles for reactors and separation processes is a fundamental step in their way towards commercialization. Extrusion techniques which are used for shaping many porous materials resulted in significant reduction of surface area in many MOF materials and thus alternative techniques are required. One alternative way to shape soft materials is to use a technique coming from molecular gastronomy and biology; the calcium alginate method. For this method, a slurry of the porous material and sodium alginate is prepared and then dropwise put in contact with calcium chloride solution forming spheres. Forming particles with both suitable diffusion and mechanical properties and without significant reductions in surface area, many operating variables must be tuned and optimized. This publication presents the results obtained showing the effects of varying several process variables of the alginate method for shaping UiO-66 MOF. Characterization in terms of surface area and other surface methods, force required to break particles (crushing strength) and measurement of isotherms of carbon dioxide. With this method we have produced MOF particles with crushing strength similar to alumina or silica) and with only 10% of reduction in surface area and adsorption capacity.

Introduction

A metal-organic framework (MOF) is a coordination network where metal ions or metal clusters binds to multifunctional organic ligands extending in 2 or 3 dimensions yielding a framework potentially containing a high fraction of voids [1-3]. This material class has gained tremendous interest due to its properties and the ease of designing. Surface areas going far beyond other porous materials and surface properties with multifaceted applications make them usable in many potential areas, such as catalysis, gas storage, gas separation, drug delivery [4-7]. It is worthy to say that some drawbacks in realising the utilization of several MOF materials are the cost [8, 9] (mostly driven by the cost of the organic linkers) and their stability [10].

The discovery of novel MOF structures, their characterization and utilization in different potential applications sum up more than 8000 publications only in 2018. However, the number of publications devoted to formulation of the MOF powder into solids that can be used in chemical processes is much smaller. This is a key step in transferring MOFs to industrial environments.

The most well-known technique to formulate porous solids is extrusion [11]. For this technique, a MOF-containing paste should be prepared together with other components that ensure plastic rheological properties. Most of these binders and plasticizers are combusted or annealed at temperatures around 500 °C in air. Due to the existence of organic molecules, MOF materials cannot be processed using such standard techniques. A possibility is to use a small amount of binders that will remain in the generated solid after extrusion [12-16]. Some cases of 3D printing (fused filament) use a similar process. The main issue with remaining binders is that the extrusion is difficult to implement, and the amount of binders must be accurately selected and controlled to avoid extensive loss of surface area [17-19]. For these reason, novel techniques for manufacturing of MOF particles are required. Granulation is another technique that can be used for shaping MOFs [20-21]. Pressing without or with a small amount of binders

has also been reported [22-25]. However, there are very limited amount of industrial applications that used pressed or cast-moulded powders.

One of the interesting MOF materials is UiO-66, the first zirconium-based MOF reported, which exhibits exceptional chemical, thermal and mechanical stability compared to other known MOFs [26]. UiO-66 has a specific surface area (BET) between 1100 and 1600 m^2/g dependent on the number of defects in the structure. In air, it decomposes at around 350 °C while under vacuum the decomposition occur above 450 °C. UiO-66 also is chemically stable in boiling water and can also withstand low concentrations of H_2S, SOx and NOx [10]. It is also important to mention that the minimal shear modulus of UiO-66 MOFs is over 12 GPa [27].

One possibility to develop UiO-66 particles is using the alginate method [28]. This method of encapsulating and shaping substances is popular in areas like gastronomy [29-31] and biology [32, 33]. In this method, the MOF is mixed or encapsulated by a cross-linked biopolymer. There are several naturally-occurring substances known to form stable gels (hydrogels) in contact with a gel-inducing agent. Alginate, chitosan, and carrageenan are some of these hydrocolloid-forming polysaccharides. Hydrogel particles are produced when alginates are cross-linked with a gel-inducing agent, such as a multivalent cation. This physicochemical method is called *ionotropic gelation*.

In this work, we have studied the effect of the most important process variables to produce UiO-66 beads by the alginate method. Our targets are a small loss of surface area and very good mechanical properties without introducing significant diffusional limitations. We have studied: (a) the effect of alginate type and (b) its concentration, (c) the concentration of calcium ions as gel-inducing agent and (d) the gelation time. Moreover, (e) the effect of the size of the beads was evaluated together with (f) the activation temperature after shaping. Furthermore, the possibility of using other gel-inducing cations was evaluated. We have characterized the produced beads with respect to mechanical strength

and surface area and, in some cases, also with respect to adsorption of carbon dioxide to evaluate the effect of the shaping process on the final adsorption properties.

Material and methods

Material syntheses

Detailed Synthesis of UiO-66 (SH-55): SH-55 batch sample was synthesized by sequentially adding 3.78 g ZrCl4 (16.2 mmol), 2.86 ml 35 % HCl (32.4 mmol), and 5.39 g H2BDC (32.4 mmol) to a 250 ml conical flask containing 97.4 ml of N,N'-dimethyl formamide (1260 mmol). BDC:Zr molar ratio in the synthesis solution was 2:1. The synthesis mixture was stirred until the solution was completely transparent before being transferred to 200 mL Teflon liners and sealed in stainless steel autoclaves where it was heated to 200 °C for 20 hours. The resulting microcrystalline powder was separated from the solvent by centrifugation and dried overnight in an oven set to 60 °C.

Physical properties of alginate depend highly on its molecular structure; the average molecular weight and the ratio of guluronate (G) to mannuronate (M) along the chain. G:M ratio varies depending on the natural source [34]. Three different block types are present in alginates; M-blocks with consecutive M residues (MMMMM), G-blocks with consecutive G residues (GGGGG), and alternating M and G residues (MGMGMG). It is believed that only G-blocks and alternating MG-blocks participate in crosslinking. The G-blocks of the polymer form junctions with the G-blocks of adjacent polymer chains by reacting with multivalent cations (except for Mg^{2+}). In this way, G-blocks and MG-blocks form an ordered structure often illustrated by an egg-box model [35]. The difference in G:M ratio, sequence, G-block length and molecular weight account for the differences in resulting hydrogels [36].

Alginates with different properties (see Table 1) were used for the formulation in order to test how the M:G ratio and the molecular weight affects the mechanical strength of the beads. All alginates were purchased from FMC Biopolymer. Calcium chloride hexahydrate (>99.0 %) purchased from Sigma Aldrich was, if not otherwise stated, used as gelation agent.

The standard procedure for production of spherical beads is as follows. The MOF powder (UiO-66) was added to pre-measured amount of distilled water. The solution was stirred for some minutes before sodium alginate powder was subsequently added. MOF/alginate slurry was stirred at room temperature for at least 60 minutes in order to make the solution as homogeneous as possible. The stirred solution was then added to the gelation bath drop by drop using a pipette. The standard gelation bath was prepared by dissolving 2.0 % (w/v) of $CaCl_2 \cdot 6H_2O$ (91.3 mM) in distilled water if not otherwise noted. The curing is done using an at least 10-fold excess of calcium chloride. Standard gelling time was 30 minutes. Beads were subsequently washed with distilled water three times for 10 minutes to remove the excess amount of calcium and chloride ions in the beads. For washing, a 10-fold volume of water were used. Washed beads were dried at 60 °C in an air oven overnight. To perform a comparable dehydration procedure removing water from the shaping and most of the adsorbed water, beads were activated before characterization and the compression test. A standard activation temperature of 135 °C under vacuum was used if not otherwise stated. Figure 1 shows how the average particles look when they are just prepared and after activation.

Characterization methods

Compression Test

3 to 4 beads having similar shape and size were selected for the compression test in order to minimize the deviation in mechanical stability. The machine used was Zwick/Roell Z250 universal test machine equipped with 500 N load cell. One bead at a time was placed between the parallel compression plates. The lower compression plate was raised at a rate of 0.2 mm per minute while the force (in Newtons) was recorded as a function of deformation of the bead in millimeter. The output data was collected using the software TestXpert II. When each particle breaks, there is a sudden decrease of required force. The force at the moment when each particle breaks is recorded and results for the 3-4 beads are averaged and reported as the average crushing strength.

Powder X-ray Diffraction

Powder X-Ray diffraction (PXRD) patterns were collected on a Bruker D8 Discover diffractometer equipped with a focusing Ge (111) monochromator (the angle (θ) for the Ge (111) peak is 27.3˚), using Cu-Kα1 radiation ($\lambda = 1.54056$ Å) and a Bruker LYNXEYE detector. The PXRD data was obtained in reflectance Bragg-Brentano geometry over a 2θ range of 2-50˚.

Prior to measurements, all the formulated MOF samples were ground thoroughly using a mortar and subsequently pressed using a manual powder press.

Thermogravimetric Analysis – Differential Scanning Calorimetry (TGA-DSC)

TGA-DSC measurements were made with Stanton Redcroft TGA-DSC, in which ca. 30 mg of sample was loaded in a Pt-crucible. Different types of calcium alginate (without MOF) and formulated MOF sample were investigated. Samples were heated to 900 ˚C at a rate of 5 ˚C·min^{-1} (in one case, for comparison, 1 ˚C·min^{-1} was used) under a constant and simultaneous flow of both N_2 (20 mL·min^{-1}) and O_2 (5 mL·min^{-1}).

Measurements and analysis of adsorption/desorption isotherms

Nitrogen adsorption measurements were performed on a BELSORP-Mini II instrument at 77 K. In each measurement, approximately 50 mg of sample was weighed into a 9.001 cm^3 sample cell. Each sample was activated at 135 ˚C under vacuum for 2 hours prior to analysis. The conditions for this pre-treatment were chosen based on the solvent weight loss step measured by TGA. The specific surface area was estimated using the BET model of multilayer adsorption. The choice of the relative pressure (p/p_0) range for the linear fit can have severe impact on the value of the derived BET surface area. The most vital part of the method is thus choosing the "correct" range. The consistency criteria originally outlined by Rouquerol et al. were employed [37].

Upon finding a pressure range that satisfies all three criteria above, the range was fine-tuned to obtain the best linear fit (i.e. maximum R^2 value) in which the three criteria are still fulfilled.

For low pressure CO_2 uptake measurement, CO_2 sorption isotherms were obtained using a BELSORP-Max instrument over a pressure range of 0 to 100 kPa at 298.15 K. The measuring temperature was controlled by using an external water bath. Prior to measurement, samples were activated at 135 ˚C under vacuum (~2 Pa) for 180 minutes.

Scanning Electron Microscopy

SEM pictures and elemental analysis (EDX) were collected in a Hitachi SU8230 Ultra High Resolution Cold FE-SEM instrument.

Fourier Transform Infrared (FTIR) Spectroscopy techniques

Infrared spectra were recorded on a Fourier transform infrared spectrometer Vertex 80, and the spectra were acquired in transmission mode on a self-supporting pellet of powdered material.

Optical microscopy

An optical microscope Leica M205 C was used to take pictures of some of the alginate beads with and without MOF for macroscopic comparison. Images were acquired and processed using a software Leica Application Suite version 3.6.0.

Results and discussion

Effect of type of alginate used

The first tests were carried out to find the effect of the type of alginate used on critical parameters such as thermal stability and strength of the beads. Using the five different alginates listed in Table 1, beads without MOF and also beads with 90wt% (dry basis) UiO-66 were gelled using the standard conditions. The non-MOF containing calcium alginates formed were dried at 40 °C in air overnight. The TGA-DSC show that a steady weight loss accompanied by an endothermic heat flow (dehydration) happens until around 185 °C where the sudden drop in mass occurs for all five alginates. There is a slight difference in the position of the endothermic minimum between the different alginates and the total mass loss caused by dehydration; the three first alginates having their minima at a slightly higher temperature compared to the two last (with smaller M:G ratio) as well as a lower total dehydration than the two last. Also, for the first three alginates there is a clear exothermic peak just before the steep mass loss around 180 °C which can be attributed to some oxidation of the alginate by gaseous oxygen. The final steep loss of mass is due to decomposition by pyrolysis (Figure S2).

Figure 2 shows the average crushing strength of the beads prepared with the five different alginates containing UiO-66. After activation, the Manugel beads are slightly stronger than beads made with GP7450 and GP5450, which again are significately stronger than beads made with LF10/60 and LF10/60L alginates. Also the thermal stability seems to be lower for the two last alginate beads. That trend can be explained by the differences in average molecular weights and M:G ratios: the first three alginates have the highest average molecular weights. Since only G-blocks in the alginate molecules are believed to participate in intermolecular crosslinking to form hydrogels, beads are stronger when formulated using alginates with higher G-block content. This phenomenon can be observed when comparing LF10/60 with LF10/60L beads and Manugel with the GP5450 and GP7450 beads, in both groups the strongest beads are made with the alginate having the highest G block content.

Effect of alginate content in the bead

A series of beads were prepared using the standard procedure but varying the alginate/MOF ratio in the slurry. Both the alginate concentration (GP7450 or Manugel) and the amount of UiO-66 in the slurry was varied as indicated in Table 2 keeping the total volume of water constant. The dry content of MOF in the final dried beads was between about 85.0 and 97.6 wt%.

The quality and shape of the beads formed is strongly dependent on the alginate concentration used. It was found that DWL-5 with alginate concentration of 0.50 % (w/v) was tear-shaped. With alginate GP7450, the minimum concentrations needed to obtain a sphere was approximately 0.45 % (w/v) to barely form a thin layer on the bead surface. However, the dried beads show low sphericity and have wrinkles which were formed by shrinkage of beads during drying (a in Figure S4). When the concentration was increased to 0.55 % (w/v), the beads became more spherical (b in Figure S4).

Figure 3 shows the bead crushing strength as a function of alginate concentration used in the slurry (left) and also as function of alginate content in the dry bead (right). The strength of beads increases proportionally to the alginate concentration used in the MOF slurry. The dependence of alginate content in the final bead (right diagram in Figure 3) show lower correlation; it is clear that a certain amount of alginate is necessary to produce beads of a certain strength, but it is the alginate concentration in the solution from which the beads are made that mainly governs the strength of the final bead. This is shown in Table 2 by the three beads of similar sizes having 10% alginate content but made from MOF slurries having different alginate concentrations, 1.1, 1.5 and 2.0 w/v respectively. The two last samples indicate that the specific surface areas (Manugel, given in Table 4) of the beads are mainly dependent on the content of alginate in the final bead and not so much by the alginate concentration used in the precursor MOF slurry.

One of the possible explanations of the observed trend is that since the alginate is dispersed throughout the bead, the contribution from the whole structure (not only from the outer shell) contributes to

withstand the applied stress. So, when the amount of alginate increases, a greater strength is obtained. Insoluble calcium alginate is acting like a hollow three-dimensional framework throughout the bead.

Once that a good mechanical resistance is obtained, it is important to verify that the properties of the original MOF material are not severely modified. Figure 4 shows the N_2 isotherms of selected beads with different alginate content, while Table 3 displays the numerical data together with expected reduction in specific surface area from the true amount of MOF in the beads.

The differences between expected and measured values are low, showing that either structural defects or pore blocking induced by the alginate are not significant at these alginate levels. Since one Ca-ion (M=40 g/mol) substitutes two Na-ions (M=23 g/mol) in the gelling process, the change in cation should not affect the estimates for the expected surface areas significantly.

EDX analyses of the beads show that the molar Ca content is from 6 to 10% of the molar Zr content corresponding to not more than 1.5 wt% Ca in the final bead. In addition to the Ca used to cross-bind the alginate, a certain amount of additional Ca^{2+} (and Cl^-) will be adsorbed within the bead after the gelling step, so the total amount of Ca^{2+} (and Cl^-) in the final bead will be very dependent on the number and quality of the succeeding washing steps (See Table S3).

Accumulated calcium and chloride ions in the outer layer of unwashed beads did not affect the porosity as shown in Figure S7. It might be because of relatively small ionic sizes of Ca^{2+} and Cl^- ions and that N_2 is an inert gas.

Samples with the dry MOF content set to 90 wt% and varying the alginate (Manugel) concentration in order to confirm that the alginate does not affect the porosity. Both N_2 isotherms were almost identical; the alginate does not seem to affect the porosity much within the range of alginate concentration 0.5 – 2.0 %(w/v).

The increase in alginate content in the bead does not negatively affect the MOF structure within the alginate content range used in this study; both PXRD data and N_2 sorption measurement confirm this. However, one could not increase the alginate concentration and keep the dry MOF content at the same level simultaneously; in order to prepare a well-mixed MOF/alginate mixture, the viscosity of the mixture must also be considered. The viscosity of alginate solutions increases quickly and above a certain alginate concentration (typically slightly above 2.0 %(w/v)) it becomes difficult to make a mixture in which alginate and MOF powder is homogeneously distributed in the slurry.

Effect of cation concentration in gelation solution

In another series of experiments with the standard procedure for bead formation, the gelation bath was prepared with different concentrations of Ca^{2+}. The concentration range of calcium chloride used in the gelation bath is given in Table 4. After preparation, all samples were dried at 40 °C overnight in an air oven. Prior to any measurement, samples were activated at 150 °C for 2 hours in vacuum.

Using too low Ca^{2+}-ion concentration (0.2 % (w/v)) results in the formation of beads with irregular shapes (Figure 5). The sphericity improved steadily when the calcium chloride concentration was increased up to 2.0 % (w/v). For low concentrations, the process is governed by kinetics: The kinetics of bead formation is not fast enough to keep the spherical shape. Since the kinetics is proportional to the calcium ion concentration [38, 39], the sphericity of the beads improves to perfection at around 2-3 %. When the concentration is further increased to above 5.0 % (w/v), the density of the gelation bath becomes higher than the slurry; the slurry droplets then float on the surface before they sink as calcium and chloride ions in the gelation bath diffuse into the beads thus increasing the bead density. This process takes approximately 30 seconds in the 5 % gelation bath and 150 secs in the 10 % gelation bath. This caused the formation of tear-shaped beads (4th picture in Figure 6). In this case, the gelation rate was so fast that some of beads did not have time to regain their shape after their initial deformation

when entering the gelation bath. Also. as the less dense beads covered the whole surface of gelation bath and got close to each other, triplets as shown in the last picture of Figure 6 was formed.

The average strength of DWL-9 beads formulated under six different gelation conditions is shown in Figure 6. There is a linear correlation between calcium concentration from 0.2 % (w/v) to 2.0 % (w/v) in the gelation bath and the crushing strength of beads, but it levels off at higher concentrations. These observations indicate that the alginate concentration in each bead is quite low, so it does not need much calcium ions to saturate the anionic alginic acids present.

The lower crushing strengths for beads formulated in dilute calcium chloride solution (0.2 % (w/v) and 0.5 % (w/v)) is considered to be due to the irregular shape of beads.

Effect of Gelation Time

A series of experiments were carried out using the standard gelling conditions but varying the gelation time used. Table 5 gives the main experimental conditions used in this series.

Gelation time was varied from 3 minutes to overnight (ca. 14 hours). Crushing strength and gas sorption isotherms are presented in Figure 7 and 8, respectively. EDX measurement was also recorded for samples prepared with gelation times of 3 minutes, 15 minutes and overnight are shown in Figure S10.
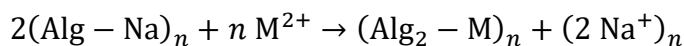
The average crushing strength was highest for 3 min samples and is slowly reduced with gelation time. However, 3 min and 5 min samples were not perfectly spherical but were slightly flat on the side which pressed towards the floor during the air drying indicating that the gelation time was too short, i.e. that the degree of cross-linking for those samples was not enough to maintain the bead framework. Bead samples that were exposed to gelling solution for 10 minutes or longer were more spherical and showed no significant reduction in sphere strength within the range studied.

The beads with gelation time of 3 min and 14 hours do not differ much in sorption isotherms (N_2 and CO_2 shown in Figure 8) indicating that the quantity of sodium ions present in the beads in contact with the Ca^{+2} solution for 3 minutes do not affect the adsorption properties of these gases. Since also the CO_2 isotherms of the two samples are similar, the interaction between CO_2 and the different metal ions present can be considered similar. The crushing strength was quite constant within the gelation time range used in this work (3 minutes to ~14 hours). However, the shape of final dried beads depends on the gelation time. The beads that were exposed to the standard gelation solution (2 %(w/v) for less than 5 minutes were not as spherical as other beads with gelation time longer than 10 minutes.

Effect of type of cation as gelation agent

Different multivalent ions were used to test their effect in the final properties of the beads. The conditions of the experiments made are summarized in Table 6. In all experiments the total charge of the cation (i.e. of Ba^{2+}, Cu^{2+}, Al^{3+}, Cr^{3+} or Zr^{4+}) was the same as the total charge of Ca^{2+} ions in the gelation solution with 2 %(w/v) of $CaCl_2 \cdot 6\ H_2O$. In order to have same overall charge, the calculated moles of the cation were multiplied by 1, 2/3 and by 1/2 for divalent, trivalent and tetravalent cations, respectively. Reaction equations for gelation between sodium alginate and multivalent cations are:
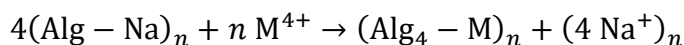
Divalent cation:

$$2(\text{Alg} - \text{Na})_n + n\ \text{M}^{2+} \rightarrow (\text{Alg}_2 - \text{M})_n + (2\ \text{Na}^+)_n$$

Trivalent cation:

$$3(\text{Alg} - \text{Na})_n + n\ \text{M}^{3+} \rightarrow (\text{Alg}_3 - \text{M})_n + (3\ \text{Na}^+)_n$$

Tetravalent cation:
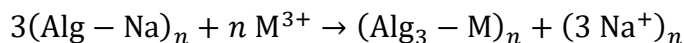
$$4(\text{Alg} - \text{Na})_n + n\ \text{M}^{4+} \rightarrow (\text{Alg}_4 - \text{M})_n + (4\ \text{Na}^+)_n$$

All beads using the different gelation agents were produced using the same alginate (Manugel).

Since the different curing cations gave beads with different shapes, comparable results could not be obtained from the crushing strength measurements. Thus, a different strategy was used. To form aluminum and zirconium cured beads, the droplets were pre-cured in a calcium chloride bath and then immediately transferred to an Al or Zr-gelation bath, where curing (and ion exchange) proceeded for 90 minutes. With this methodology, it was possible to make almost spherical Al- and Zr-alginate beads as shown in Figure 9.

The average crushing strength decreases rapidly with cations with increasing valence as shown in Figure 10. Interestingly, Cu-alginate beads were significantly weaker than Ca-alginate beads, and Cr-alginate beads were weaker than Al-alginate beads even though they have same valence (+3). This could mean that the strength of alginate gel depends on two main parameters; i) the pH and ii) electron affinity of the cation in the gelation bath.

Figure 11 shows the N_2 and CO_2 isotherms of the beads produced with the different cations. The use of Al^{3+} ions and Zr^{4+} ions did not affect the nitrogen sorption isotherms significantly. The relative ionic radius of Ca^{2+}, Al^{3+} and Zr^{4+} are 1.80 Å, 1.25 Å and 1.55 Å, respectively. The small and similar ion sizes do not seem to block the pores of the MOF.

Interestingly, the beads cross-bonded with Cu^{2+} and Al^{3+} showed a slight increase in CO_2 uptake compared to those gelled with Ca^{2+}. The dry MOF content in all the MOF-beads used in this work is 90 wt% (not taking the differences in mass of the gelling agents into consideration). One explanation for the observed slight increase in CO_2 capacity (particularly at lower partial pressures) can be a consequence of the greater electron affinity of Cu^{2+} and Al^{3+} ions in the alginate framework that could attract molecules having electron donating abilities, such as CO_2, stronger, thus results in higher uptake per mass, especially at low pressures. Additionally, the molecular weight of cations for Al^{+3} and Cu^{+2}

is smaller than in the Ca^{+2} samples and thus the amount of MOF per gram of sample is slightly smaller for the Ca^{+2} ones.

Effect of activation temperature and time

Beads produced by the standard method (DWL-9-Ca2%) were activated at three different temperatures (120 °C, 135 °C and 150 °C) for 2 hours under vacuum prior to IR measurements. An IR spectrum of MOF-powder (SH-55) activated at 150 °C was used as the adsorbent reference. In addition, alginate GP7450 was crushed and mixed with KBr to make a pellet in which the alginate was distributed as uniform as possible. The DWL-9-Ca2%, data was also collected by crushing it and mixing with KBr into a pellet. The IR spectra reported in Figure 12 summarizes the progressive dehydration of DWL-9-Ca2%, enhancing the OH stretching regions.

The IR spectra of DWL-9-Ca2% is dominated by an intense and broad band centered at 3380 cm^{-1} due to OH stretching modes that can be ascribed to water adsorbed in the alginate. For UiO-66, the band in this region refers to intercrystallite physisorbed water condensed inside the crystal cavities [40]. The peak at 3674 cm^{-1} corresponds to a small fraction of isolated OH groups present on the external surfaces of the microcrystals. This peak becomes sharper when the sample is treated at higher temperature.

Higher activation temperature removes more water from the material and results in relative decrease of the broad band centered at 3380 cm^{-1} and an increase in intensity and sharpness of the peak of isolated OH groups due to loss of hydrogen bonding. At 120 and 135 °C the second peak around 3669 cm^{-1} that reduces in intensity and becomes a shoulder at 150 °C. This additional peak also related to isolated OH groups that is not observed in the IR spectrum of pure UiO-66. We therefore assign his peak to stretching mode of OH groups of the cross-bonded alginate framework. The reduction in intensity at 150 °C can be a consequence of the partly degradation occurring at this temperature.

Unlike DWL-9-Ca2%, the IR spectrum of UiO-66 activated at 150 °C for 2 hours shows no broad band around 3000-3600 cm^{-1}; meaning that there is no water left at after this treatment and only free OH groups left. However, the formulated bead activated in the same condition (blue curve) still possesses a broad band after the same treatment. This is most probably due to both adsorbed water and inherent OH-groups in the alginate molecules. The IR spectrum of alginate precursor (green curve in (a)) has a broad band that overlaps quite well with the band observed in the formulated beads.

A series of TGA experiments were carried out to study the dehydration in more detail. Figure 13 show the mass traces for long-term TGA experiments where the set-temperatures were 120, 135 and 150 °C, respectively. Tre trend is clear: First there is a rapid dehydration going on which depth is strongly dependent on the set-temperature used. The rapid dehydration is followed by a much slower dehydration that only slowly seems to level off and reach a steady plateau sometime after these TGA experiments were terminated. In the IR spectra the slow dehydration is shown as a slow reduction in the area of the broad peak centered around 3380 cm^{-1} (Figure S9).

Table 8 shows the weight loss data from the TGA experiments. The dehydration rate is increasing with an increase in the temperature both in the initial loss of water as in the longer-term mass loss. We believe the fast part of the dehydration is due to a rapid loss of free water within the alginate framework and the MOF pores, while the slow following loss is due to the slow removal of adsorbed water from the strongly hydrophilic alginate framework and also from the hydrophilic pore surfaces (the Zr-oxide cluster) within the MOF.

During the slow dehydration period, mass was consistently lost, and heat was generated. Since desorption alone is endothermic, the heath flow observed most probably is due to degradation of alginate which is exothermic [41]. Degradation was visible; the color of beads changed when increasing the temperature from 120 to 150 °C (Figure 14). The color change was mainly happening during the

slow dehydration period since beads activated at 150 °C for only two hours still had an off-white surface. (Figure S10).

Mechanical crushing strength measurements of one identical sample of beads (DWL-9-Ca2%) was measured after activation at four different activation conditions: The results are given in Figure 15. The difference in average crushing strength between beads activated at 120 °C and 135 °C was very small; indicating the alginate is quite thermally stable up to 135 °C. Higher activation temperatures led to reduced crushing strength: a decrease from 20.9 N to 16.2 N when the activation temperature was increased from 135 °C to 150 °C. We attribute this 22.5 % decrease in crushing strength to the fact that more alginate was decomposed at the higher temperature.

Nitrogen and CO_2 isotherms were measured on DWL-9-Ca2% samples after activation for 2 hours at 120 °C or 150 °C, respectively. Precursor MOF powder (SH-55) having undergone similar treatments was also measured as a reference and results are reported in Figure 16. The volume of nitrogen adsorbed at $p/p_0 = 0.5$ is 303 cm^3g^{-1}, 255 cm^3g^{-1}, 253 cm^3g^{-1} for SH-55, DWL-9 (150 °C) and DWL-9 (120 °C), respectively. The decrease in volume is 15.8 % and 16.5 % and fits well with expected value since the dry MOF content in DWL-9 is 85 wt%. No significant difference between 120 and 150 °C was observed indicating that the additional water physisorbed in the beads does not affect the porosity of the material. The small amount of water that can be removed from 120 to 150 °C must then be within the hydrophilic alginate framework and not within the pores of the MOF crystals. Since nitrogen is an inert gas that does not interact with OH groups in water molecules, CO_2 uptake measurement was conducted. However, the difference in CO_2 uptake between these two activation temperatures was indistinguishable (Figure 16b).

The results suggest that there is no significant difference between activation at temperatures between 120 °C and 150 °C in terms of adsorption isotherms, even though the IR spectra show clear differences. That broad band caused mainly by hydrogen-bonded water and OH groups of alginate moieties do not

block the cavities in UiO-66. The main effect of a highest activation temperature (150 ℃) is a reduction in crushing strength of the beads which is most likely a consequence of partly degradation of the alginate framework.

Effect of Size of Beads

As pressure drop over fixed beds is directly related to the size of the beads used in the columns, we also studied the effect on adsorption and mechanical stability of different bead diameters. A series of beads was prepared using different nozzles having a variation in aperture diameters as described in the supplementary material. Beads were made from SH-55/alginate suspension (DWL-10) with alginate Manugel (1.5 % (w/v)) using the standard procedure. The beads were activated at 135 °C for 2 hours prior to crushing strength measurement, N_2 and CO_2 sorption measurements.

The beads varied in spherical diameters between 1.8 mm and 2.9 mm. As seen in Figure 17, the average crushing strength increases significantly with the size of beads. As the bead diameter increases, the contact area both on top and bottom of the bead becomes larger when the bead starts to deform upon the external stress. For the bigger beads, the force per unit area will then be smaller and result in an increased crushing strength.

Regarding the adsorption properties of beads with the same composition but different size, there is no significant difference as shown in Figure 18. This indicates that despite the size becoming larger there is no blocking of pores using this methodology, at least within the range of diameters studied (1.835 mm to 2.905 mm).

Conclusions

We have studied the properties of beads of UiO-66 shaped by the alginate method. We have varied the most important possible process parameters aiming to determine the effect of shaping in mechanical properties and adsorption equilibrium. The range of parameters selected have experimental constrains like densities and viscosities that are practical to handle by scaled processes. We also have kept the alginate content in the final bead lower than 15 wt% since one of our main aim is to produce MOF-beads having only a small reduction in specific surface area compared to the precursor MOF powder.

We determined that alginates with high G-block content are superior to alginates with low G-block content in terms of mechanical strength. Molecular weight of alginate also plays an important role in thermal stability. In this work, alginate with M:G ratio of 40:60 and molecular weight of 240-300 kDa resulted in the best properties.

Gelation times above 15 minutes in 2 %(w/v) (0.09 mM) calcium chloride did not increase the gel strength, and a washing time of 10 minutes was found to be enough for the 2-3 mm beads studied to not affect the specific surface area measured after activation. These parameters were found to be optimal for optimized sphericity and for maximizing the throughput of MOF-bead production.

All of the alginates used in this work start degrading at relatively low temperature (~70 °C). Air drying prior to the activation should not be above 60 °C. Above 135 °C, the alginate degradation slightly reduces the crushing strength of the beads and when activation temperature exceeds 150 °C, the gel strength decreases rapidly. It was found that activation temperature of 120 - 135 °C was optimal for the UiO-66/alginate beads.

The strength of the strongest UiO-66/alginate beads produced are comparable with commercially available silica and alumina beads (~20N) and should therefore be suitable for use in adsorption columns and other fixed bed reactors. Because of the low penalty in the specific surface area of the MOF/alginate beads, we believe the method is a general and promising method for shaping of water-

stable MOFs (and other porous materials). An additional advantage is that this method is easily implemented in small scale but is also easily scalable.

Acknowledgments

References

1. Yaghi, O. M.; O'Keffe, M.; Ockwig, N. W.; Chae, H. K.; Eddaoudi, M.; Kim, J. Reticular synthesis and design of new materials. Nature 423 (2003) 705-714. https://doi.org/10.1038/nature01650

2. Ferey, G. Hybrid porous solids: Past, present, future. Chem. Soc. Rev. 37 (2008) 191-214. https://doi.org/10.1039/B618320B

3. Horike, S.; Shimomura, S.; Kitagawa, S. Soft porous crystals. Nat. Chem. 1 (2009) 695-704. https://doi.org/10.1038/nchem.444

4. Jiao, L.; Wang, Y.; Jiang, H. L.; Xu, Q. Metal-organic frameworks as platforms for catalytic applications, Adv. Mater. 30 (2018) 1703663. https://doi.org/10.1002/adma.201703663

5. Morris, R.; Wheatley, P. S. Gas storage in nanoporous materials. Angew. Chem., Int. Ed. 47 (2008) 4966-4981. https://doi.org/10.1002/anie.200703934

6. Bastin, L.; Barcia, P. S.; Hurtado, E. J.; Silva, J. A. C.; Rodrigues, A. E.; Chen, B. L. A microporous metal-organic framework for separation of CO_2/N_2 and CO_2/CH_4 by fixed-bed adsorption. J. Phys. Chem. C 112 (2008) 1575-1581. https://pubs.acs.org/doi/10.1021/jp077618g

7. Simon-Yarza, T.; Mielcarek, A.; Couvreur, P.; Serre, C. Nanoparticles of metal-organic frameworks: On the road to in vivo efficacy in biomedicine. Adv. Materials 30 (2018) 1707365. https://doi.org/10.1002/adma.201707365

8. Sathre, R.; Masanet, E. Prospective life-cycle modelling of a carbon capture and storage system using metal-organic frameworks for CO_2 capture. RSC Advances 3 (2013) 4964-4975. 10.1039/C3RA40265G

9. DeSantis, D.; Mason, J. A.; James, B. D.; Houchins, C.; Long, J. R.; Veenstra, M. Techno-economic analysis of metal-organic frameworks for hydrogen and natural gas storage. Energy & Fuels 31 (2017) 2024-2032. https://pubs.acs.org/doi/abs/10.1021/acs.energyfuels.6b02510

10. Low, J. J.; Benin, A. I.; Jakubczak, P.; Abrahamian, J. F.; Faheem, S. A.; Willis, R. R. Virtual high throughput screening confirmed experimentally: Porous coordination polymer hydration. *J. Am. Chem. Soc.* 131 (2009) 15834-15842. https://pubs.acs.org/doi/10.1021/ja9061344

11. Perego, C.; Villa, P. Catalyst Preparation Methods. Catal. Today 34 (1997) 281-305. https://doi.org/10.1016/S0920-5861(96)00055-7

12. Kusgens, P.; Zgaverdea, A.; Fritz, H. G.; Siegle, S.; Kaskel, S. Metal-organic frameworks in monolithic structures. J. Am. Chem. Soc. 93 (2010) 2476-2479. https://doi.org/10.1111/j.1551-2916.2010.03824.x

13. Hong, W. Y.; Perera, S. P.; Burrows, A. D. Manufacturing of metal-organic framework monoliths and their application in CO_2 adsorption. Micro. Mesopor. Mater. 214 (2015) 149-155. https://doi.org/10.1016/j.micromeso.2015.05.014

14. Masala, A.; Vitillo, J. G.; Mondino, G.; Martra, G.; Blom, R.; Grande, C. A.; Bordiga. S. Conductive ZSM-5-Based Adsorbent for CO_2 Capture: Active Phase vs Monolith. Ind. Eng. Chem. Res. 56 (2017) 8485-8498. https://pubs.acs.org/doi/abs/10.1021/acs.iecr.7b01058

15. Sultan, S.; Abdelhamid, H. N.; Zou, X.; Mathew, A. P. CelloMOF: Nanocellulose enabled 3D printing of metl-organic frameworks. Adv. Funct. Mater. 29 (2019) 1805372. https://doi.org/10.1002/adfm.201805372

16. Halevi, O.; Tan, J. M. R.; Lee, P. S.; Magdassi, S. Hydrolitically stable MOF in 3D-printed structure. Adv. Sustainable Syst. 2 (2018) 1700150. https://doi.org/10.1002/adsu.201700150

17. Grande, C. A.; Águeda, V. I.; Spjelkavik, A.; Blom, R. An Efficient Recipe for Formulation of Metal-organic Frameworks. Chem. Eng. Sci. 124 (2015) 154-158.

18. N. Casas, J. Schell, R. Blom, M. Mazzotti. A parametric study of a PSA process for pre-combustion CO2 capture. Sep. Purif. Technol. 112 (2013) 34– 48

19. J. Zheng, X. Cui, Q. Yang, Q. Ren, Y. Yang, H. Xing. Shaping of ultrahigh-loading MOF pellet with a strongly anti-tearing binder for gas separation and storage. Chem. Eng. J. 354 (2018) 1075-1082.

20. J. Ren, N.M. Muskoya, H.W. Langmi, A. Swartbooi, B.C. North, M. Mathe. A more efficient way to shape metal-organic framework (MOF) powder materials for hydrogen storage materials. Int. J. Hydrog. Energy 40 (2015) 4617-4622.

21. A.H. Valekar, K-H. Cho, U-H. Lee, J. S. Lee, J. W. Yoon, Y.K. Hwang, S.G. Lee, S.J. Cho, J-S. Chang. Shaping of porous metal-organic framework granules using mesoporous p-alumina as binder. RSC Adv. 7 (2017) 55767.

22. S. Cavenati, C.A. Grande, A.E. Rodrigues, C. Kiener, U. Mueller. Metal Organic Framework Adsorbent for Biogas Upgrading. Ind. Eng. Chem. Res. 47 (2008) 6333 – 6335.

23. G.W. Peterson, J.B. DeCoste, T. Grant Glover, Y. Huang, H. Jasuja, K.S. Walton. Effect of palletization pressure on te physical and chemical properties of the metal-organic frameworks Cu3(BTC)2 and UiO-66. Microp. Mesop. Mater. 179 (2013) 48-53.

24. A. H. Valekar, K-H. Cho, U-H. Lee, J. S. Lee, J. W. Yoon, Y.K. Hwang, S.G. Lee, S.J. Cho, J-S. Chang. Shaping of porous metal-organic framework granules using mesoporous p-alumina as binder. RSC Adv. 7 (2017) 55767.

25. M.I. Hossain, J.D. Cunningham, T.I. Becker, B.E. Grabicka, K.S. Walton, B.D. Rabideau, T. Grant Glover. Impact of MOF defects on the binary adsorption of CO2 and water in UiO-66. Chem. Eng. Sci., 203 (2019) 346-357.

26. Cavka, J. H.; Jakobsen, S.; Olsbye, U.; Guillou, N.; Lamberti, C.; Bordiga, S.; Lillerud, K. P. A New Zirconium Inorganic Building Brick Forming Metal Organic Frameworks with Exceptional Stability. J. Am. Chem. Soc. 130 (2008) 13850-13851. https://pubs.acs.org/doi/abs/10.1021/ja8057953

27. Wu, H.; Yildirim, T.; Zhou, W. Exceptional mechanical stability of highly porous zirconium metal-organic framework UiO-66 and its important implications. J. Phys. Chem. Lett. 4 (2013) 925-930. https://pubs.acs.org/doi/10.1021/jz4002345

28. Spjelkavik, A. I.; Aarti; Divekar, S.; Didriksen, T.; Blom. R. Forming MOFs into Spheres by Use of Molecular Gastronomy Methods. Chem., Eur. J. 20 (2014) 8973-8978. https://doi.org/10.1002/chem.201402464

29. Russin, T. A. Getting creative with hydrocolloids. Food Technol. 64 (2010) 58–65.

30. This, H. Solutions are solutions, and gels are almost solutions. Pure Appl. Chem. 85 (2013) 257–276. https://doi.org/10.1351/PAC-CON-12-01-01

31. Barham, P.; Skibsted, L. H.; Bredie, W. L. P.; Frøst, M. B.: Møller, P.; Risbo, J.; Snitkjær, P.; Mortensen, L. M. Molecular gastronomy: A new emerging scientific discipline. Chem. Rev. 110 (2010) 2313 –2365. https://pubs.acs.org/doi/10.1021/cr900105w

32. Pandolfi, V.; Pereira, U.; Dufresne, M.; Legallais, C. Alginate-based cell microencapsulation for tissue engineering and regenerative medicine. Current Pharma. Des. 23 (2017) 3833-3844. https://doi.org/10.2174/1381612823666170609084016

33. Kamperman, T.; Karperien, M.; Le Gac, S.; Leijten, J. Single-cell microgels: Technology, challenges, and applications. Trends in Biotechnology 36 (2018) 850-865. https://doi.org/10.1016/j.tibtech.2018.03.001

34. Haug, A. Fractionation of Alginic Acid. Acta Chem. Scand. 13 (1959) 601-603.

35. Fu, S.; Thacker, A.; Sperger, D. M.; Boni, R. L.; Buckner, I. S.; Velankar, S.; Munson, E. J.; Block, L. H. Relevance of Rheological Properties of Sodium Alginate in Solution to Calcium Alginate Gel Properties, AAPSPharmSciTech 12 (2011) 453-460. https://dx.doi.org/10.1208%2Fs12249-011-9587-0

36. George, M.; Abraham, T. E. Polyionic hydrocolloids for the intestinal delivery of protein drugs: Alginate and chitosan — a review. J. Contr. Release 114 (2006) 1-14. https://doi.org/10.1016/j.jconrel.2006.04.017

37. Rouquerol, F.; Rouquerol, J.; Sing, K. Adsorption by powders and porous solids, Academic press, 1999, pp 166-169.

38. Lee, P.; Rogers, M. A. Effect of calcium source and exposure-time on basic caviar spherification using sodium alginate. Int. J. Gastro. and Food Sci. 1 (2012) 96-100. https://doi.org/10.1016/j.ijgfs.2013.06.003

39. Lee, B.-B.; Ravindra, P.; Chan, E.-S. Size and shape of calcium alginate beads produced by extrusion dripping. Chem. Eng. Techn. 36 (2013) 1627-1642. https://doi.org/10.1002/ceat.201300230

40. Valenzano, L.; Civalleri, B.; Chavan, S.; Bordiga, S.; Nilsen, M. H.; Jakobsen, S.; Lillerud, K. P.; Lamberti, C. Disclosing the Complex Structure of UiO-66 Metal Organic Framework: A Synergic Combination of Experiment and Theory. Chem. Mater. 23 (2011) 1700-1718. https://pubs.acs.org/doi/abs/10.1021/cm1022882

41. Zhang, J.; Ji, Q.; Shen, X.; Xia, Y.; Tan, L.; Kong, Q. Pyrolysis products and thermal degradation mechanism of intrinsically flame-retardant calcium alginate fibre. Poly. Degrad. Stab. 96 (2011) 936-942. https://doi.org/10.1016/j.polymdegradstab.2011.01.029

List of Tables

Table 1: Types of alginate used for the formulation.

Name	Viscosity (1%)	Molecular Weight	M:G ratio
Protanal GP7450	600 – 800 mPa·s	Ca. 380 – 400 kDa	45:55
Protanal GP5450	200 – 400 mPa·s	Ca. 280 – 350 kDa	45:55
Protanal LF10/60L	40 – 60 mPa·s	Ca. 175 – 220 kDa	60:40
Protanal LF10/60	20 – 70 mPa·s	Ca. 140 – 200 kDa	30:70
Manugel GMB	110 – 270 mPa·s	Ca. 240 – 300 kDa	40:60

Table 2 The quantities used during synthesis, the composition of the final beads and their crushing strengths.

Sample	Alginate Conc. [%(w/v)]	Water [mL]	Alginate powder [mg]	MOF powder [g]	Alginate content (dry) [wt%]	Average bead size (mm)	Mean Force (N)
DWL-5*	0.5	10	50	2.0	2.4	2.61	4.6±0.1
DWL-2*	1.0	10	100	2.0	4.8	2.54	9.0±0.8
DWL-9-1.1%*	1.1	10	111	1.0	10.0	2.75	11.9±0.7
DWL-9-1.4%*	1.4	10	143	1.0	12.5	2.71	16.0±0.7
DWL-9-1.8%*	1.8	10	180	1.0	15.0	2.77	19.9±2.0
DWL-11-2%	2.0	10	200	1.0	16.7	-	-
DWL-16-M1.5%[†]	1.5	10	150	1.35	10.0	2.74	16.5±0.4
DWL-16-M2.0%[†]	2.0	10	200	1.8	10.0	2.93	24.4±1.0

*Using alginate GP7450. [†] Using alginate Manugel.

Table 3: Comparison between the expected decrease in N_2 isotherms and the measured value at $p/p_0 = 0.5$.

	MOF content (dry) [wt%]	Expected decrease in N_2 isotherms [%]	Measured decrease in adsorbed N_2 at $p/p_0 = 0.5$. [%]	BET [$m^2 \cdot g^{-1}$] (% Decrease relative to SH-55)
SH-55	100	--	--	1241 (--)
DWL-5	97.6	2.4	4.8	1191 (4.0)
DWL-2	95.2	4.8	6.9	1160 (6.5)
DWL-11-2%	85	15	16.1	1029 (17.1)
DWL-16-M1.5%	90	10	9.4	1117 (10.0)
DWL-16-M2.0%	90	10	11.6	1084 (12.7)

Table 4: Experimental details for the series of beads produced using different Ca^{2+} concentrations in the gelation bath.

Sample	Batch (dry content)	Alginate type (concentration)	Conditions
DWL-9-Ca0.2%			$CaCl_2 \cdot 6\ H_2O$, 0.2 % (w/v), 0.5 hrs
DWL-9-Ca0.5%			$CaCl_2 \cdot 6\ H_2O$, 0.5 % (w/v), 0.5 hrs
DWL-9-Ca1.0%			$CaCl_2 \cdot 6\ H_2O$, 1.0 % (w/v), 0.5 hrs
DWL-9-Ca2.0%	SH-55 (85 wt%)	GP7450 (1.8 % (w/v))	$CaCl_2 \cdot 6\ H_2O$, 2.0 % (w/v), 0.5 hrs
DWL-9-Ca5.0%			$CaCl_2 \cdot 6\ H_2O$, 5.0 % (w/v), 0.5 hrs
DWL-9-Ca10.0%			$CaCl_2 \cdot 6\ H_2O$, 10.0 % (w/v), 0.5 hrs

Table 5. Main parameters used in this experiment.

MOF batch samples used	SH55
Dry MOF content (wt%)	90
Alginate type (concentration)	Manugel (2 % (w/v))
Washing time	15 minutes
Drying condition	40 °C overnight (air)
Activation condition	135 °C for 2 hours (vacuum)
Gelation bath	$CaCl_2 \cdot 6\ H_2O$ (2 %(w/v))
Gelation time [min]	3, 5, 10, 15, 30, 60, 120, 180, 270, 840

Table 6: Different cations with their source used in this work as well as the pH measured in the gelation baths of each cation for the given concentration.

Ion	Source	pH (23 °C)	Concentration in gelation solution
Ca^{2+}	$CaCl_2 \cdot 6\ H_2O$	6.1	2 %(w/v) (0.09 M)
Ba^{2+}	$Ba(NO_3)_2$	-	Corresponding moles of
Cu^{2+}	$CuSO_4 \cdot 5\ H_2O$	5.6	substance (0.09 M)
Al^{3+}	$Al(NO_3)_3 \cdot 9\ H_2O$	3.4	Corresponding moles of
$Cr(OH)^{2+}$, Cr^{3+}	$Cr(NO_3)_3 \cdot 9\ H_2O$	1.7	substance multiplied by 2/3 (0.06 M)
	$Zr(SO_4)_2 \cdot 4\ H_2O$	1.3	Corresponding moles of
Zr^{4+}	$ZrOCl_2 \cdot 8\ H_2O$	1.3	substance multiplied by
	$ZrO(NO_3)_2 \cdot x\ H_2O$	1.4	1/2 (0.045 M)

Table 7: The weight loss of alginates with various cations at different temperatures.

	% Weight loss at 135 °C	% Weight loss at 150 °C	% Weight loss at 200 °C
Ca^{2+}	2.27	2.91	9.72
Al^{3+}	4.39	6.37	24.17
Zr^{4+} / $Zr(SO_4)_2$	10.59	13.24	26.03
Zr^{4+} / $ZrOCl_2$	2.63	4.59	30.07

Table 8: The weight loss of DWL-9-Ca 2% at three different temperatures. Weight loss when the final temperature was reached and 12 hours after that point in each experiment are shown.

Set-temperature [°C]	Weight loss when the set-temperature is reached [wt%]	Additional weight loss after 12 hrs. [wt%]
120	5.0	0.6 %
135	8.1	1.0 %
150	10.4	1.2 %

List of Figures

Figure 1: MOF beads in the gelation solution (left) and after activation (right)
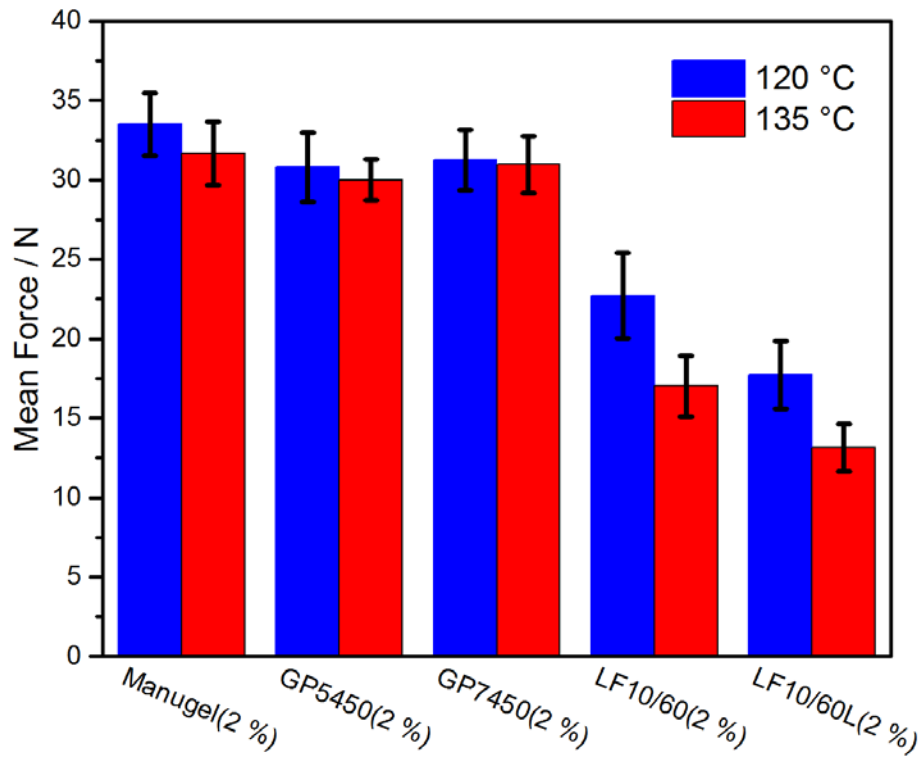
Figure 2: Average crushing force for beads formulated using different alginates. Numbers in parenthesis corresponds to the alginate concentration. Activation temperature before the crushing strength measurement were 120 °C (blue bars) and 135 °C (red bars).
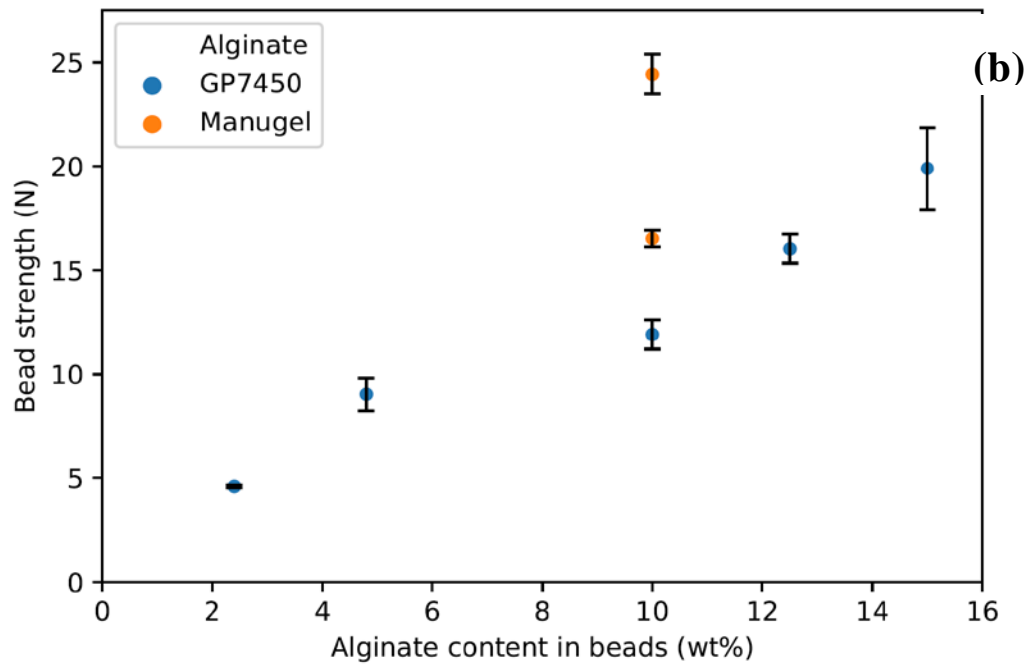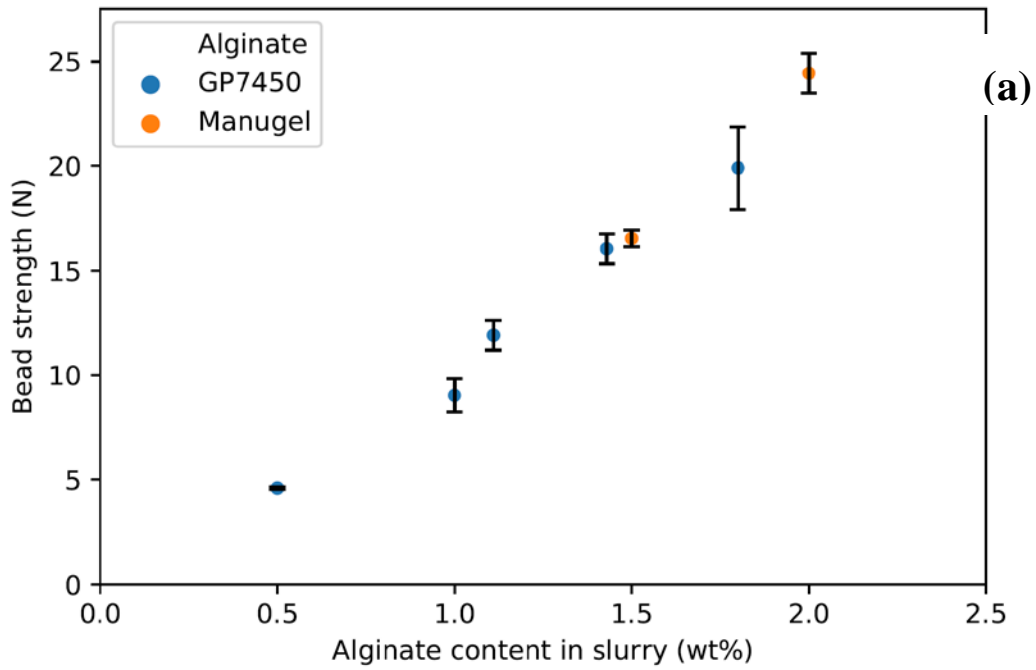
Figure 3: Average crushing strength force for beads made using different alginate concentrations (a) and for different alginate content in the dried bead (b) based on the data given in Table 3.
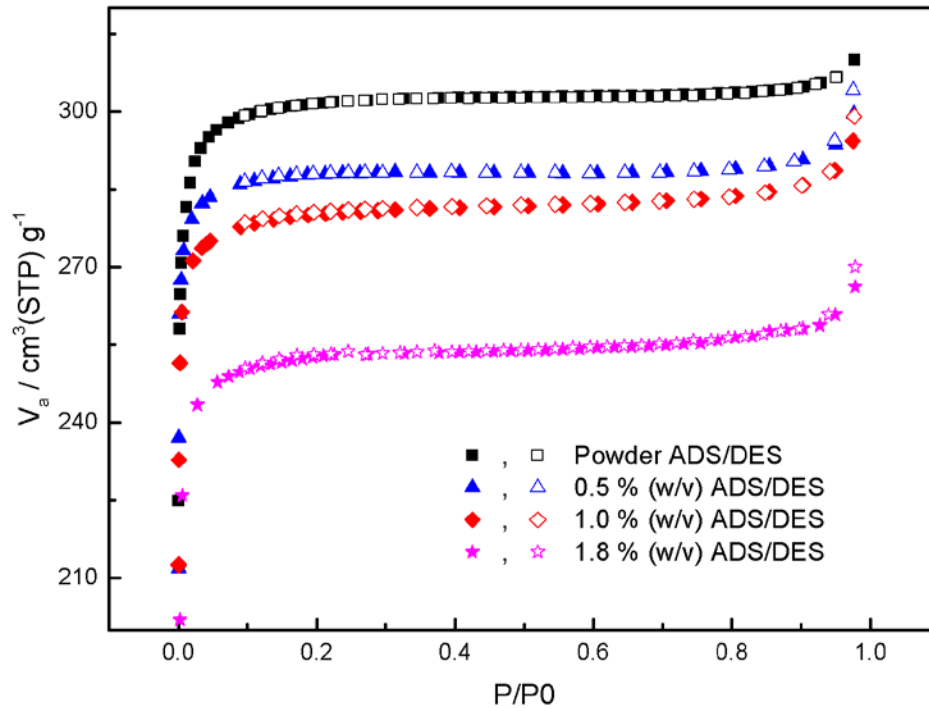
Figure 4. Adsorption/desorption N_2 isotherms at 77K of three samples prepared with different alginate concentrations. Isotherms for unformulated powder are shown as a reference value.

Figure 5: Different shapes of beads obtained for different concentration of calcium cations in the gelation bath: DWL-9-Ca0.2% (left), DWL-9-Ca0.5% (second) and DWL-9-Ca2.0% (middle). Tear-shaped beads and "triple-bead" of DWL-9-Ca10.0% (right).
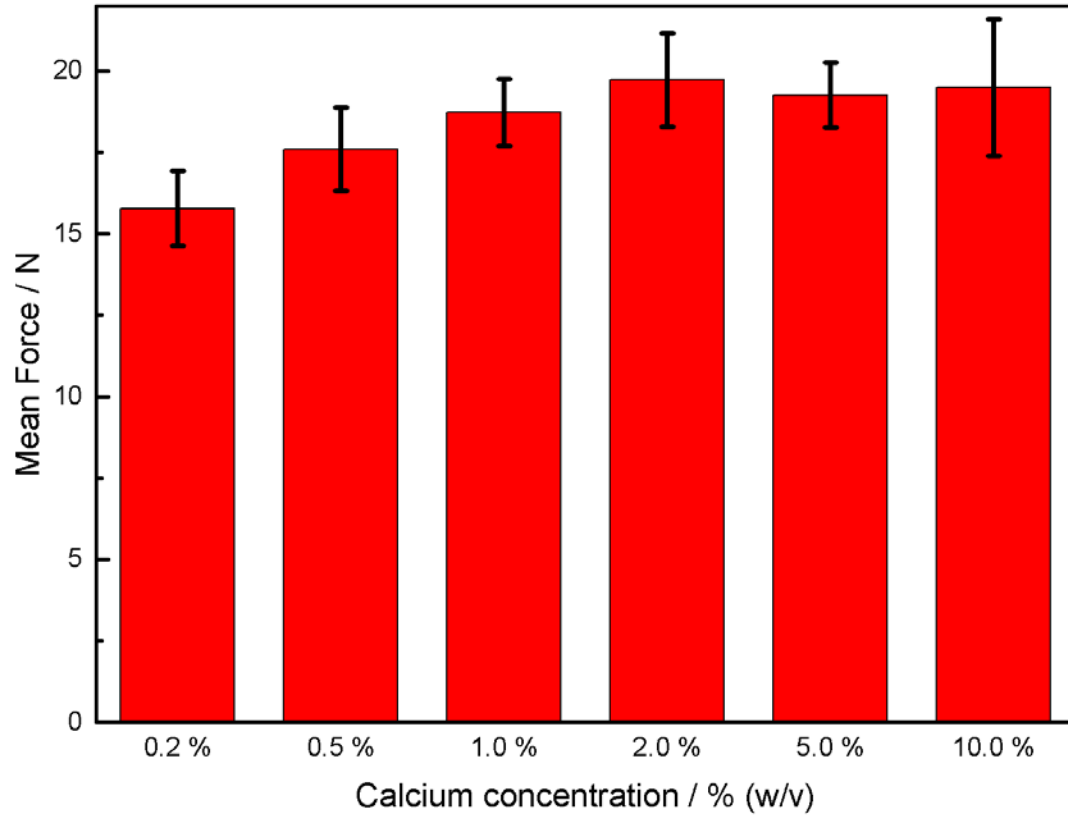
Figure 6: Averaged crushing force of DWL-9 beads formulated with different calcium concentrations.
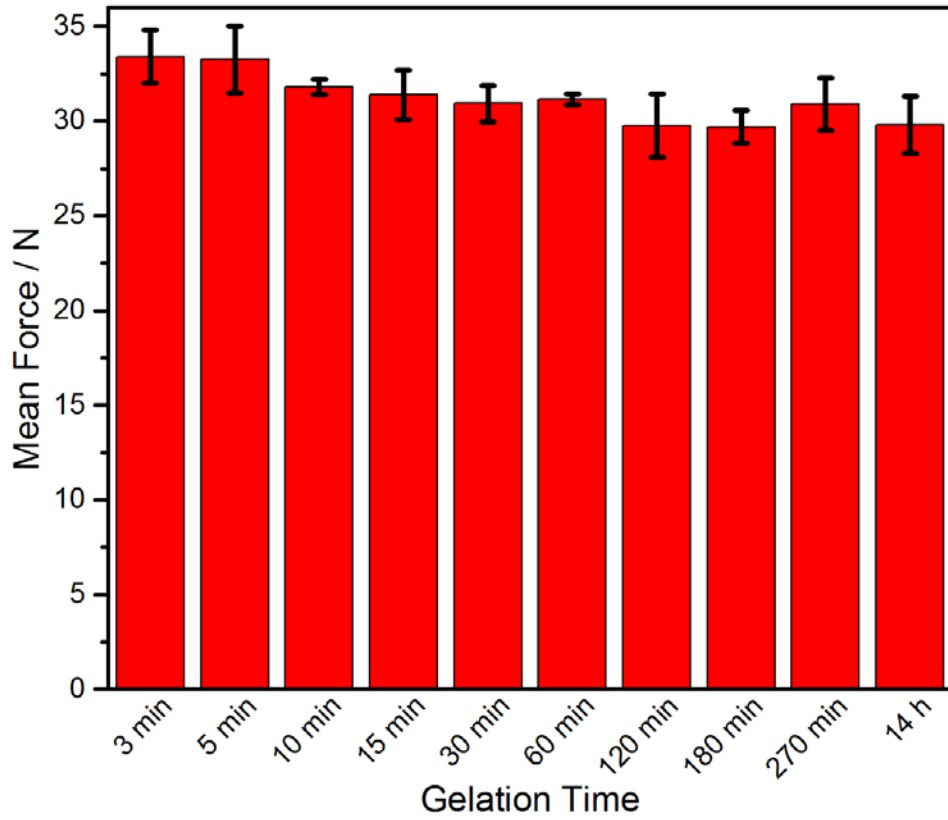
Figure 7. Averaged crushing force as a function of gelation time.
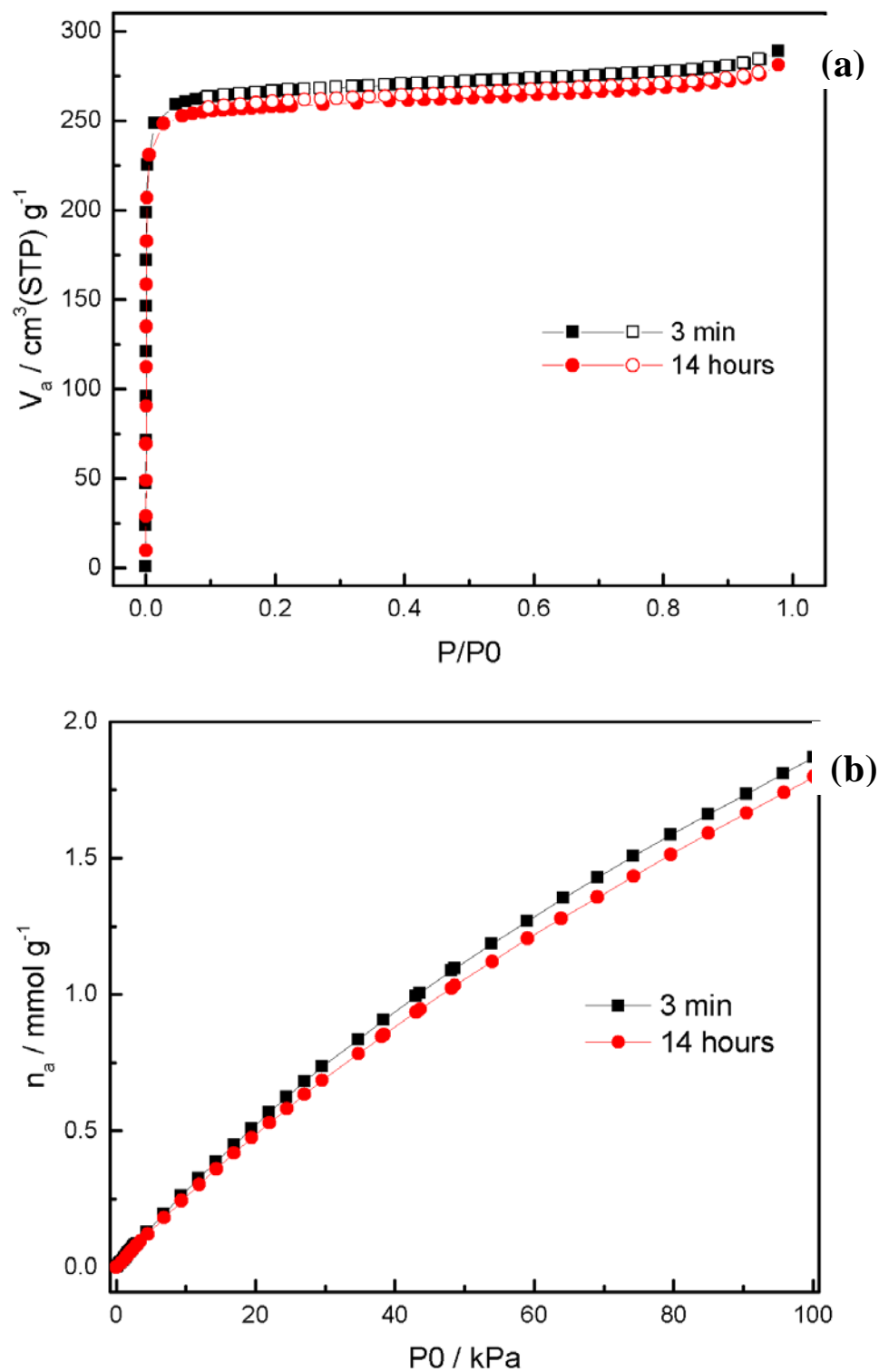
Figure 8: Nitrogen sorption isotherm at 77K (a) and CO_2 isotherms at 298 K (b) on DWL-11.

Figure 9: Top, from left to right: Cu-beads, Al-beads and Zr-beads. After activation at 120 °C for 2 hours under vacuum. Bottom, from left to right: Ca-bead, Cu-bead, Al-bead and Zr-bead.
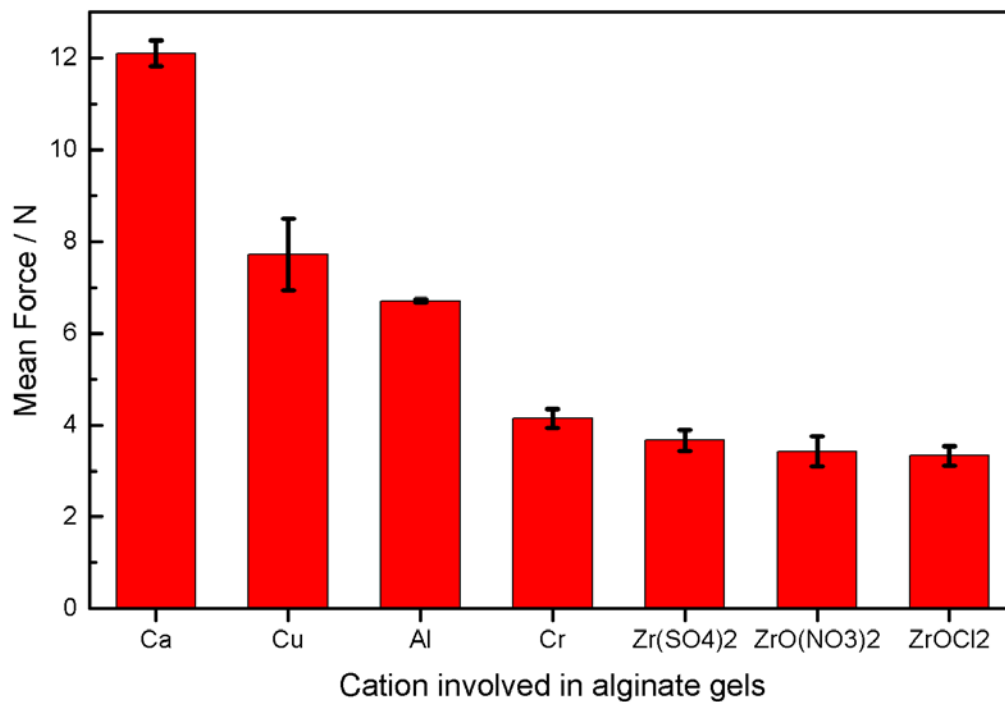
Figure 10: Averaged crushing force of alginates formed with different cations. Activated at 120 °C for 2 hours.
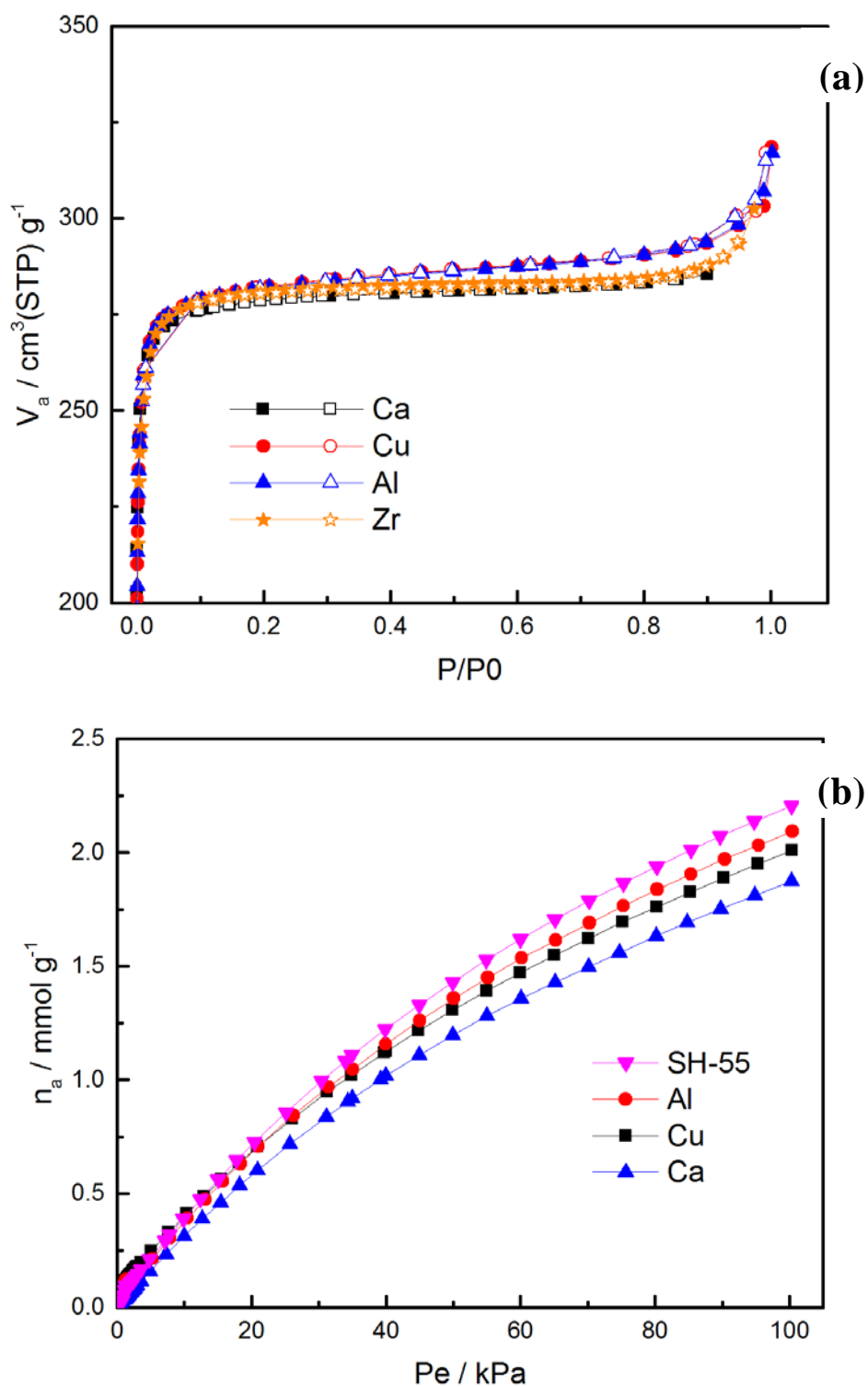
Figure 11: (a) Nitrogen sorption isotherms at 77K for beads formulated with different cations. (b) CO_2 uptake at 298K up to 1 bar. MOF powder (SH-55) plotted as reference. The dry MOF contents in other beads are 90 wt%.
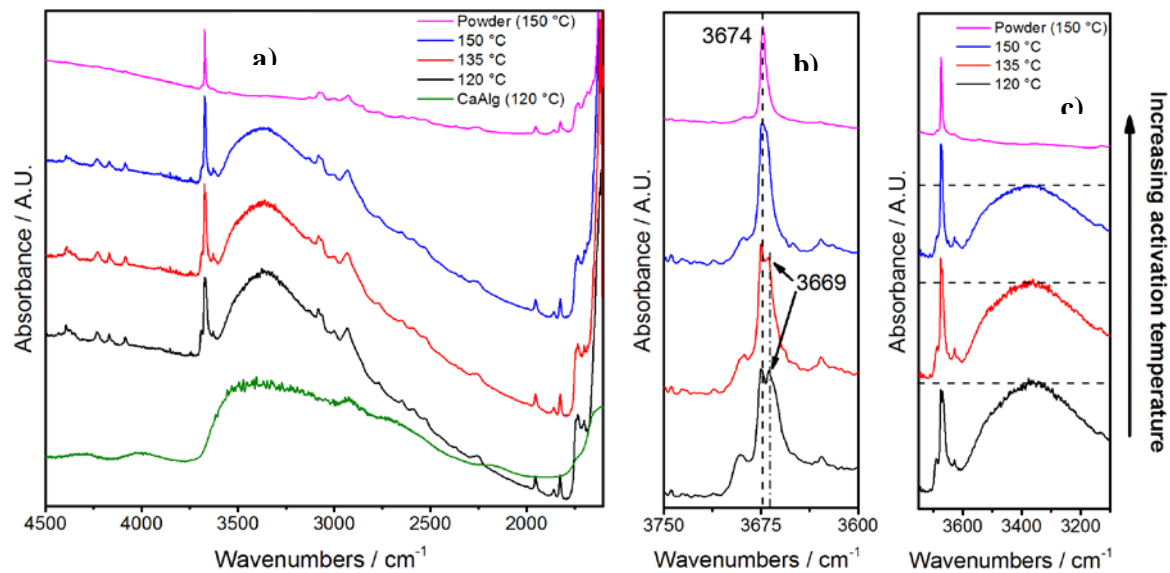
Figure 12: The IR spectra of batch powder UiO-66 (purple), DWL-9-Cl2% activated at different temperatures (black, red and blue) and alginate GP7450 (green). (a) entire spectrum, (b and c) OH stretching regions.
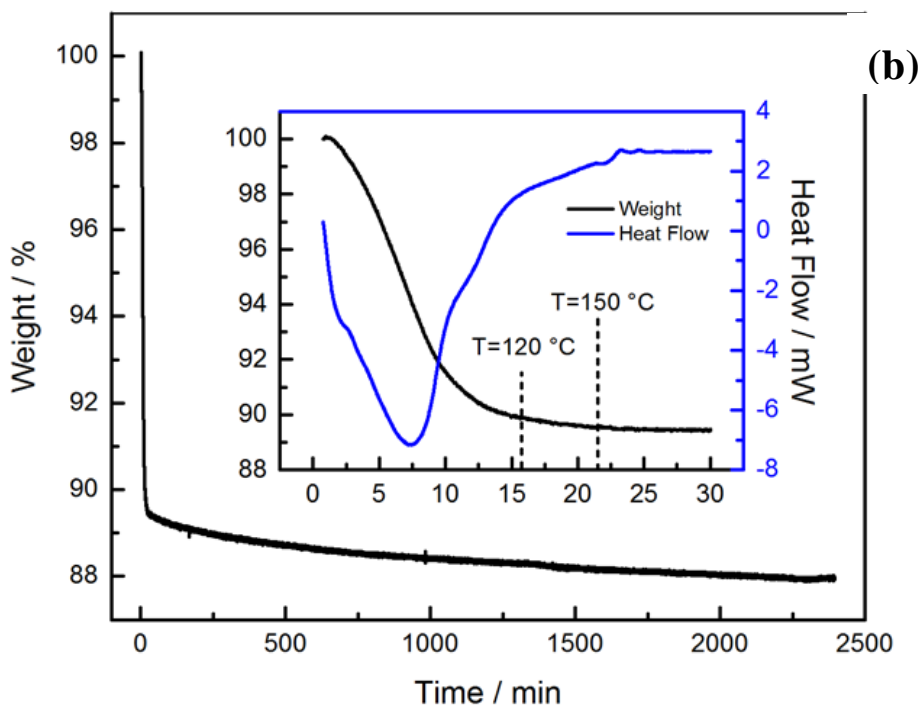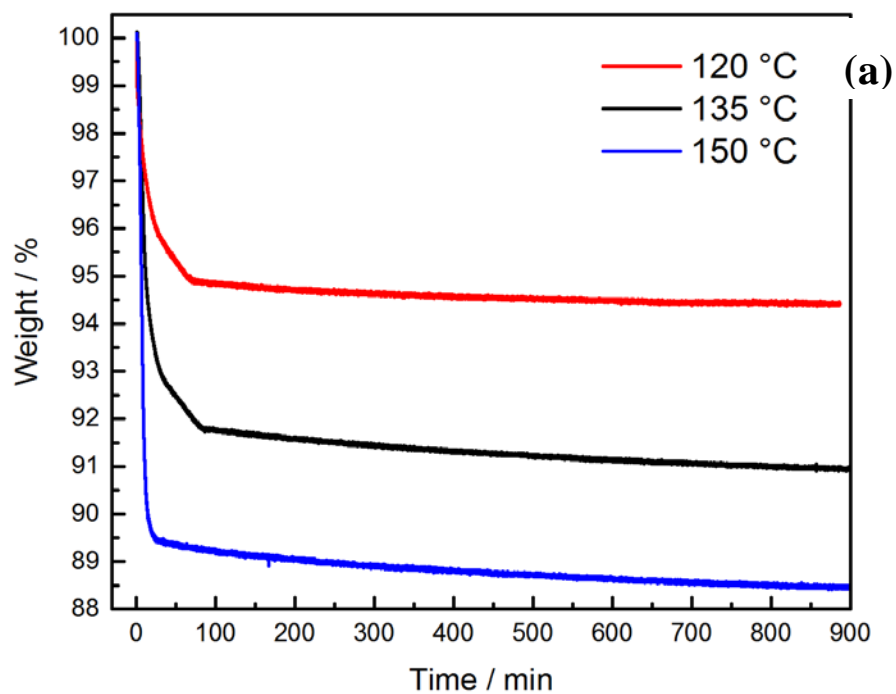
Figure 13: TGA data of DWL-9-1.8% at three different activation temperatures a) TGA data of DWL-9-1.8% at three different activation temperatures; 120, 135 and 150°C. b) More details of TGA activation of DWL-9-1.8% at 150°C showing that stable mass is still not reached after 2500 min. Insert: TGA and DSC details for the first 30 minutes showing the heat flow during the initial phase of the activation
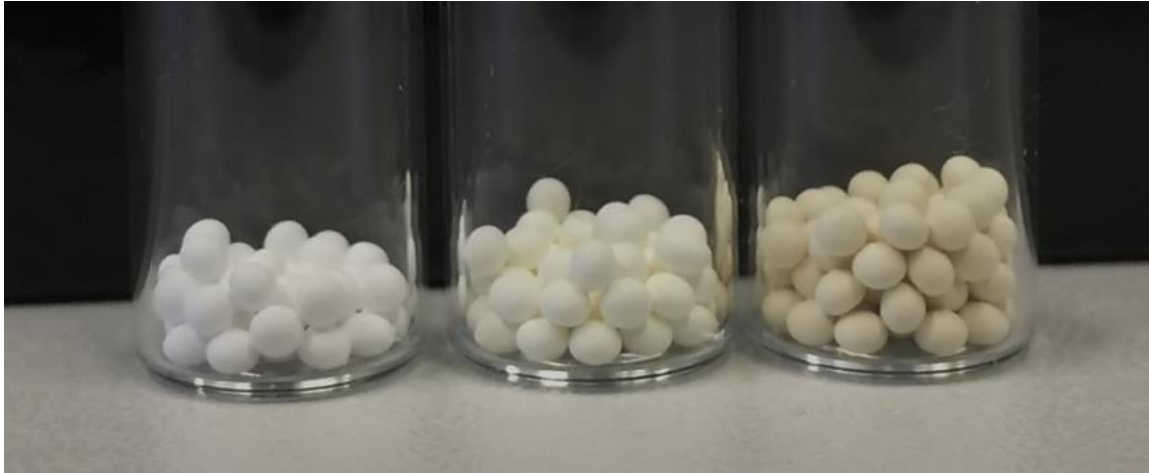
Figure 14: DWL-9-1.8% activated overnight at three different temperatures (from left to right, 120 °C, 135 °C and 150 °C).
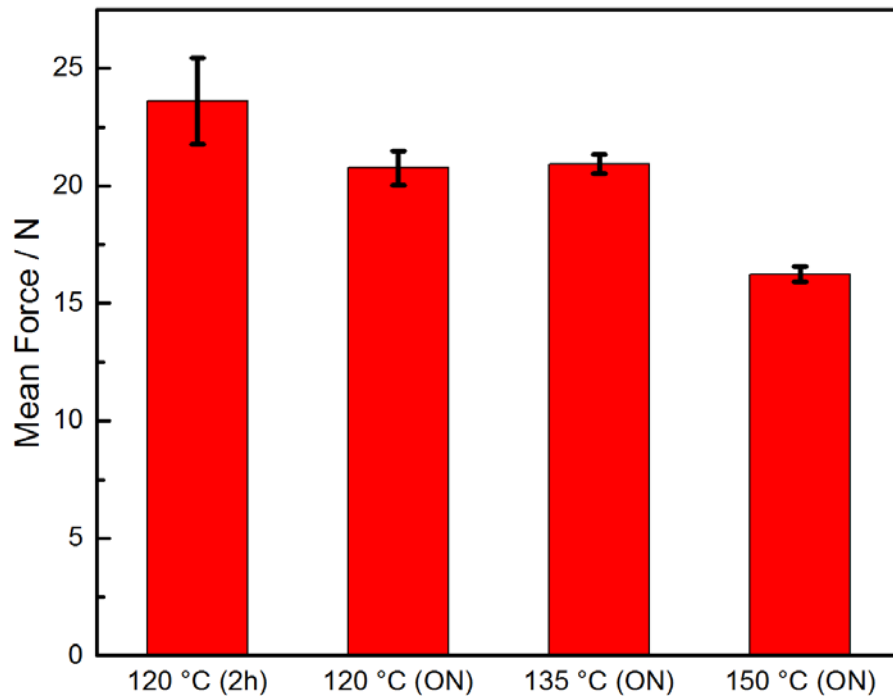

Figure 15: Average crushing strength of DWL-9-1.8% after 4 different activation conditions: activation at 120 °C for 2 hours, 120 °C overnight, 135 °C overnight, 150 °C overnight. Red bars illustrate the mean value and the error bars indicate the difference between the maximum and the minimum value.
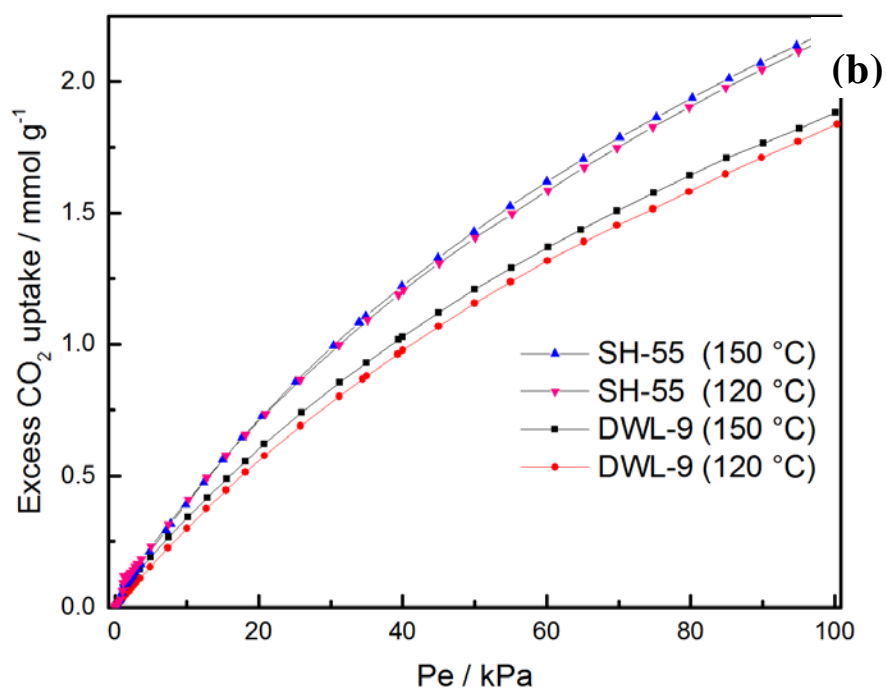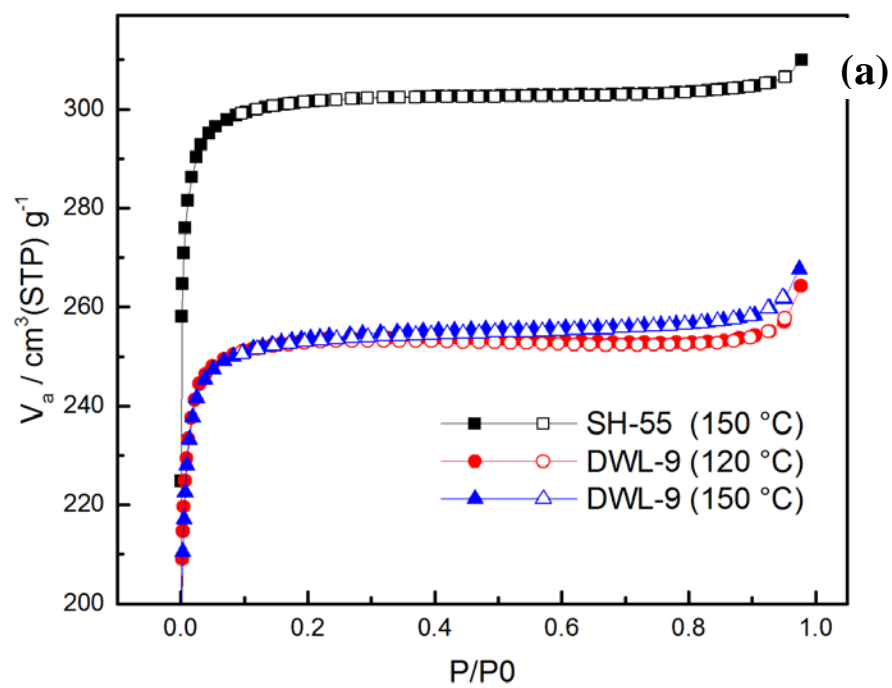
Figure 16: Nitrogen adsorption isotherm at 77K (a) and CO_2 uptake at 298 K (b) on powder (SH-55) and on beads (DWL-9) activated at two different temperatures: 120 °C and 150 °C.
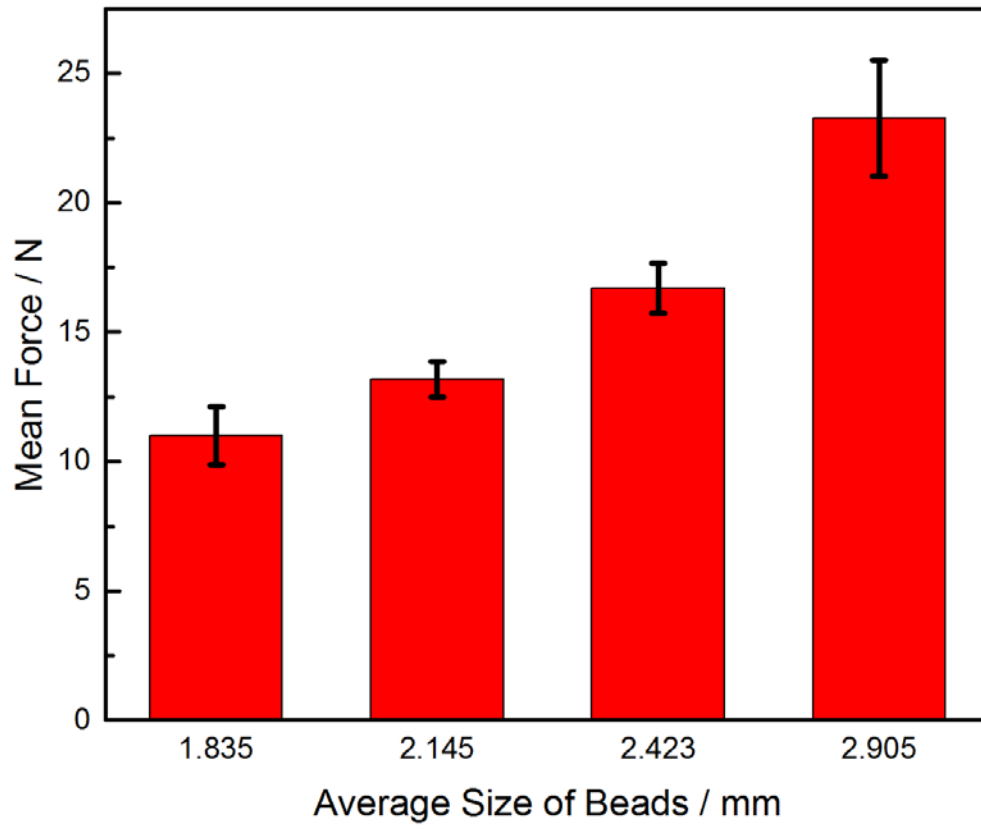
Figure 17: Average crushing strength for particles with different diameters of DWL-10 beads.
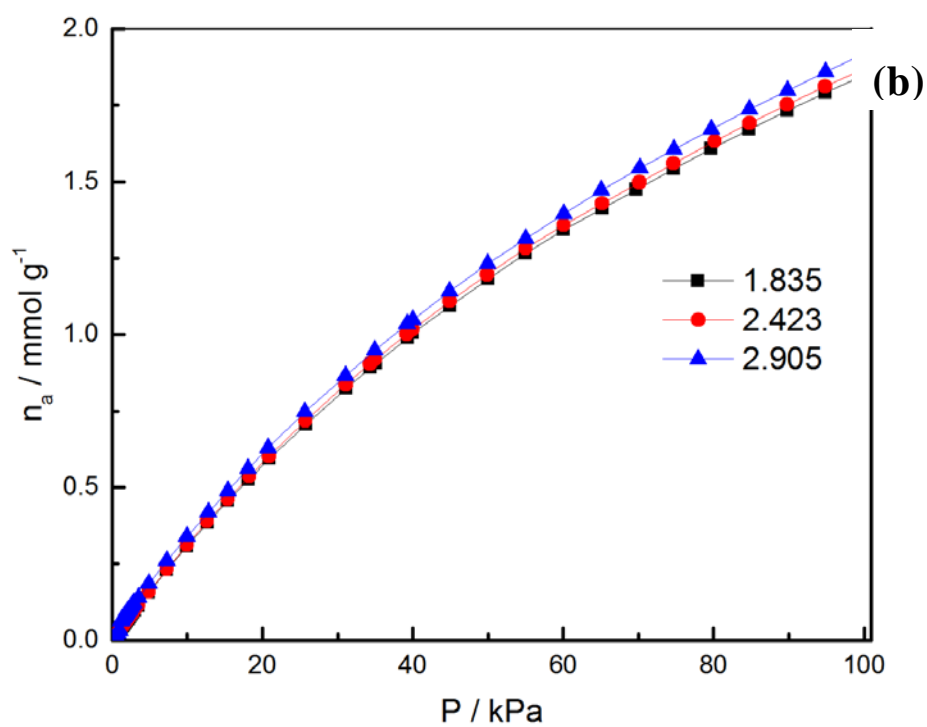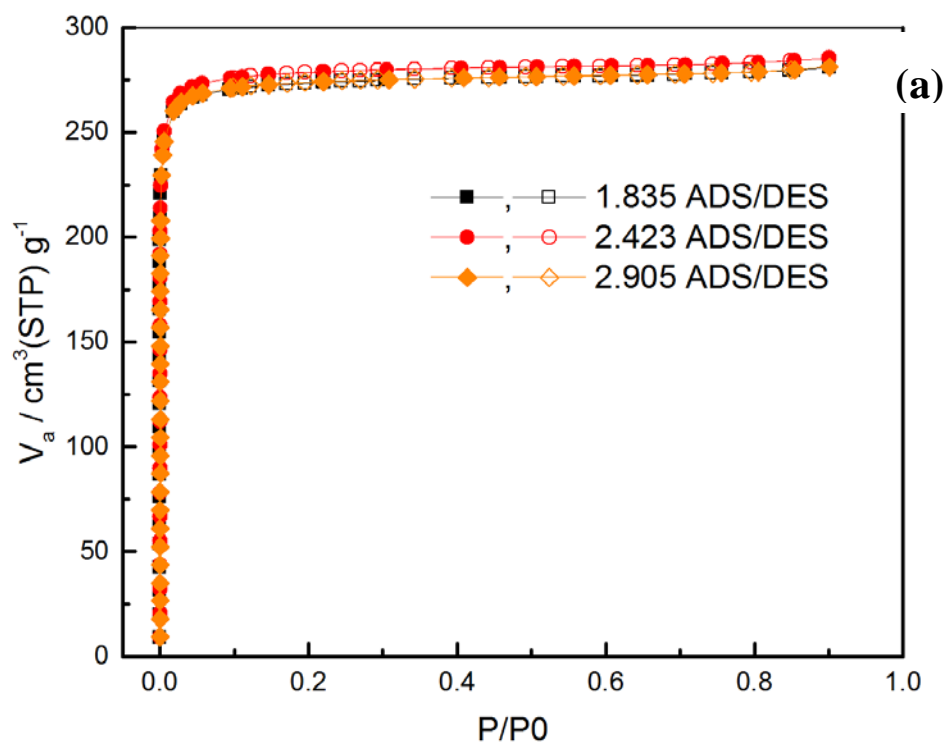
Figure 18: Nitrogen adsorption isotherms at 77K (a) and CO_2 uptake at 298 K (b) on beads with different average diameters